

Selivanovaite, $\text{NaTi}_3(\text{Ti,Na,Fe,Mn})_4[(\text{Si}_2\text{O}_7)_2\text{O}_4(\text{OH,H}_2\text{O})_4] \cdot n\text{H}_2\text{O}$, a new rock-forming mineral from the eudialyte-rich malignite of the Lovozero alkaline massif (Kola Peninsula, Russia)

YAKOV A. PAKHOMOVSKY¹, TARAS L. PANIKOROVSKII^{1,2}, VICTOR N. YAKOVENCHUK¹, GREGORY YU. IVANYUK¹, JULIA A. MIKHAILOVA¹, SERGEY V. KRIVOVICHEV^{1,2,*}, VLADIMIR N. BOCHAROV³ and ANDREI O. KALASHNIKOV¹

¹ Kola Science Centre, Russian Academy of Sciences, 14 Fersman Street, Apatity 184200, Russia

*Corresponding author, e-mail: s.krivovichev@spbu.ru

² Department of Crystallography, Institute of Earth Sciences, Saint-Petersburg State University, University Emb. 7/9, 199034 St. Petersburg, Russia

³ Geo Environmental Centre “Geomodel”, Saint-Petersburg State University, Ul’yanovskaya Str. 1, St. Petersburg 198504, Russia

Abstract: Selivanovaite, $\text{NaTi}_3(\text{Ti, Na, Fe, Mn})_4[(\text{Si}_2\text{O}_7)_2\text{O}_4(\text{OH,H}_2\text{O})_4] \cdot n\text{H}_2\text{O}$, is a new titanosilicate of the murmanite group (seidozerite supergroup). It is triclinic, $P\bar{1}$, $a = 8.673(5)$, $b = 8.694(3)$, $c = 12.21(1)$ Å, $\alpha = 92.70(5)$, $\beta = 108.46(7)$, $\gamma = 105.40(4)^\circ$, $V = 833(1)$ Å³, $Z = 2$ (from single-crystal diffraction data); $a = 8.673(5)$, $b = 8.694(1)$, $c = 12.21(1)$ Å, $\alpha = 92.70(5)$, $\beta = 108.52(1)$, $\gamma = 105.42(1)^\circ$, $V = 833(1)$ Å³, $Z = 2$ (from powder diffraction data). The mineral was found in drill cores of medium-grained trachtyoid eudialyte-rich malignite of the Lovozero eudyalite complex at Mt. Alluaiv, at the horizon 900–1000 m above the Baltic Sea level. The rock consists mainly of euhedral microcline-perthite, nepheline and mangano-eudialyte crystals cemented by fine-acicular aegirine. Minor rock-forming minerals include sodalite, natrolite, magnesioarfvedsonite, and selivanovaite (up to 10 modal %). Characteristic accessory minerals are lamprophyllite, murmanite, loparite-(Ce), a pyrochlore-group mineral, thorite, anatase, baryte, rhabdophane-(Ce), pyrrhotite, chalcopyrite, pyrite, chlorbartonite, djerfisherite, sphalerite, and löllingite. Selivanovaite forms platy metacrysts (up to 8 mm in diameter) with numerous poikilitic inclusions of aegirine and magnesioarfvedsonite. It is dark-orange, with a vitreous lustre and a brownish-white streak. The cleavage is perfect on $\{001\}$ and weak on $\{110\}$, the fracture is stepped. Mohs hardness is 3. In transmitted light, the mineral is brown; pleochroism and dispersion were not observed. Selivanovaite is biaxial (+), $\alpha = 1.79(1)$, $\beta = 1.81(1)$, $\gamma = 1.87(1)$ (589 nm), $2V_{\text{meas}} = 40(5)^\circ$, $2V_{\text{calc}} = 57.3^\circ$. The optical orientation is $Z^{\wedge}c = 5\text{--}10^\circ$. The calculated and measured densities are 3.34 and 3.15(3) g · cm⁻³, respectively. The mean chemical composition determined by electron microprobe is: Na₂O 5.45, MgO 0.59, Al₂O₃ 0.04, SiO₂ 25.55, K₂O 0.63, CaO 1.68, TiO₂ 31.17, MnO 2.64, FeO 6.63, ZrO₂ 2.31, Nb₂O₅ 6.69, with H₂O 17.0 wt% (determined by the Penfield method), giving a total of 100.38 wt%. The empirical formula calculated on the basis of Si = 4 atoms per formula unit (apfu) is $(\text{Na}_{1.65}\text{Mn}_{0.35}\text{Ca}_{0.28}\text{Zr}_{0.18}\text{Mg}_{0.14}\text{K}_{0.13})_{\Sigma 2.73}(\text{Ti}_{3.67}\text{Fe}_{0.78}^{3+}\text{Nb}_{0.47}\text{Al}_{0.01})_{\Sigma 4.93}[\text{Si}_4\text{O}_{19.72}] \cdot 8.87\text{H}_2\text{O}$. The simplified formula based upon the crystal-structure refinement is $\text{NaTi}_3(\text{TiNaFeMn}_{0.5}\square_{0.50})_{\Sigma 4}[(\text{Si}_2\text{O}_7)_2\text{O}_4(\text{OH})_2(\text{H}_2\text{O})_2] \cdot n\text{H}_2\text{O}$ or, taking into account chemical variations, $\text{NaTi}_3(\text{Ti, Na, Fe, Mn})_4[(\text{Si}_2\text{O}_7)_2\text{O}_4(\text{OH,H}_2\text{O})_4] \cdot n\text{H}_2\text{O}$. The mineral slowly dissolves in cold 10% HCl. The strongest X-ray powder-diffraction lines [listed as d in Å (J) (hkl)] are: 11.43(1 0 0)(0 0 1), 6.37(25)(-1 1 1), 5.73(15)(0 0 2), 4.208(16)(-2 1 1), 3.108(35)(2 -2 1), 3.043(20)(-1 0 4), and 2.596(17)(0 1 4). The crystal structure of selivanovaite is closely related to those of murmanite-group minerals and consists of the HOH-layers with the composition $[\text{N}_2\text{M}_5\text{Si}_4\text{O}_{18}(\text{OH})_3]$ ($M = \text{Ti, Nb, Fe and Mn}$, $N = \text{Na, K, Ca, Mn, Mg and Zr}$) connected by additional N -octahedra with H₂O molecules between them. The mineral is named in honour of Dr. Ekaterina A. Selivanova (b. 1967), from the Kola Science Centre of the Russian Academy of Sciences, for her contribution to the mineralogy of alkaline complexes.

Key-words: selivanovaite; new mineral; seidozerite supergroup; titanosilicate; crystal structure; eudialyte; malignite; Lovozero massif; Kola Peninsula.

1. Introduction

Layered titanosilicates or heterophyllosilicates with Si₂O₇ groups constitute one of the most diverse groups of minerals with the modular type of structure (Ferraris *et al.*, 2004). Belov & Organova (1962) were the first who

emphasized the analogy between the crystal structures of micas and ‘titanium micas’ (= heterophyllosilicates, Ferraris *et al.*, 1996), and the modular approach to these minerals has been developed in detail by Egorov-Tismenko & Sokolova (1987, 1990), Ferraris (1997, 2008a) and Sokolova (2006; see also Sokolova & Cámara, 2017, for

references). Ferraris (2006, 2008b) and Ferraris *et al.* (2008) pointed out that heterophyllosilicates might be of interest not only from the mineralogical, but also from the material science point of view, since the heterophyllosilicate layer may serve as a basis for a wide range of functionalized structural units with interesting physical and chemical properties. The present classification approved by the International Mineralogical Association (Sokolova & Cámara, 2017) recognizes forty-five mineral species of the seidozerite supergroup that consists of the rinkite, bafertsite, lamprophyllite, and murmanite groups.

Until this work, the murmanite group (Sokolova & Cámara, 2017) included ten titanosilicates, most of which were discovered in the Lovozero alkaline massif (Table 1). By analogy with other seidozerite-supergroup minerals, these heterophyllosilicates are based upon HOH triple layers or TS blocks (TS=titanosilicate), where an octahedral layer (O) is sandwiched between two heteropolyhedral H layers. Minerals of the murmanite group differ from each other by the composition of I-block constituents that fill the interlayer space between titanosilicate (TS) blocks (Sokolova & Cámara, 2017). Titanosilicate block is a fundamental structural block that demonstrates exceptional stability in a wide interval of PT conditions and, for instance, is retained during transformations of lomonosovite into murmanite (Lykova, 2015) and murmanite into vigrishinite (Pekov *et al.*, 2012).

While most of the murmanite-group minerals are relatively rare, lomonosovite and murmanite play the role of rock-forming minerals in nepheline syenites, foidolites and pegmatites of the Lovozero massif (up to 15 modal %). Herein we describe selivanovaite, a new member of the seidozerite supergroup, which locally occurs as a rock-forming mineral of eudialyte-rich malignites of the Lovozero massif. It was found during 3D mineralogical mapping of the Alluaiv site of the Lovozero loparite–eudialyte deposit (Kalashnikov *et al.*, 2016) and named in honour of Dr. Ekaterina A. Selivanova (b. 1967) from the Geological Institute of the Kola Science Centre of the Russian Academy of Sciences, for her contribution to mineralogy of alkaline complexes, especially for the discovery of fourteen new mineral species in Kola peninsula and the study of layered titanosilicates (Selivanova *et al.*, 2008).

Both mineral and mineral name have been approved by the Commission on New Minerals, Nomenclature and Classification of the International Mineralogical Association (IMA 2015-126). Type material is deposited in the collections of the Mineralogical Museum of St. Petersburg State University, Russia, under catalogue number 1/19649 and in the Geological and Mineralogical Museum of the Geological Institute of the Kola Science Centre, Apatity, Russia, under catalogue number GIM 7538.

2. Occurrence

The Lovozero massif of nepheline syenite–foidolites (Fig. 1a) is, with an area of about 650 km², the second world largest alkaline massif after the Khibiny one. It intruded through the Archaean granite-gneiss and the Devonian

Table 1. Chemical composition (wt%) of selivanovaite

Oxide	mean	min	max	SD*	Probe standard
H ₂ O**	17.0				
Na ₂ O	5.45	4.06	7.17	1.58	Lorenzenite
MgO	0.59	0.41	0.70	0.16	Pyrope
Al ₂ O ₃	0.04	0.00	0.11	0.06	Pyrope
SiO ₂	25.55	23.38	27.83	2.23	Diopside
K ₂ O	0.63	0.17	1.28	0.58	Wadeite
CaO	1.68	1.35	2.34	0.57	Apatite
TiO ₂	31.17	26.77	36.95	5.23	Lorenzenite
MnO	2.64	2.29	2.89	0.31	MnCO ₃
Fe ₂ O ₃	6.63	3.10	10.94	3.97	Hematite
ZrO ₂	2.31	2.01	2.71	0.36	Zircon
Nb ₂ O ₅	6.69	6.04	7.02	0.56	Nb metal
Total	100.38				

* Standard deviation.

** Determined by Penfield method.

tuff-basalt strata 362 Ma ago (Korchak *et al.*, 2011) and forms regular subhorizontal layers of trachytoid foyaite–malignite (“lujavrite”) and ijolite–urtite rock series (Fig. 1c). These layers are divided into two complexes – differentiated (bottom) and eudyalite (top), which differ by the eudialyte content, nepheline–syenite–foidolite proportion and thicknesses of individual sublayers of these rocks (Gerasimovsky *et al.*, 1966; Bussen & Sakharov, 1972; Kalashnikov *et al.*, 2016).

The most studied part of the Lovozero differentiated complex contains seven sharply bounded rhythms of nepheline syenite–foidolites, and in each of these rhythms ijolite–urtite gradually transforms to foyaite–malignite from the bottom to top (Pakhomovsky *et al.*, 2014; Kalashnikov *et al.*, 2016). At the rhythm contacts, there are narrow layers (0.1–0.4 m) of loparite-rich (up to 60 modal %) malignite–shonkinite (within the foyaite top of the lower rhythm) and ijolite–melteigite (within the foidolite bottom of the upper rhythm). The Lovozero eudyalite complex is a non-rhythmical coarse-layered stratum-like body (50–400 m thick) comprising eudialyte-rich malignite and shonkinite (“eudialyte lujavrite”) with various (mangano)eudialyte contents (up to 95 modal % and 12 modal % as the average content). Besides eudialyte itself, ore minerals of the eudyalite complex include loparite-(Ce), lomonosovite–murmanite–selivanovaite series, and lovozerite-group minerals with their contents varying inversely to the content of (mangano)eudialyte.

The Alluaiv set of the giant Lovozero loparite–eudialyte (Ta-Nb-REE-Zr) deposit (Fig. 1b, Fig. 1c) accommodates mainly eudialyte-rich malignite (12 modal % of (mangano)eudialyte on average) and loparite–eudialyte-rich foyaite (4 modal % of loparite and 6 modal % of (mangano)eudialyte). (Mangano)eudialyte grains may contain relics of primary parakeldyshite (commonly in foyaite and sporadically in malignite). A significant part of eudialyte malignite is enriched in lomonosovite and murmanite (2.5 modal % on average). In addition, within the eudialyte malignite strata, there are irregularly distributed lenses of ijolite–urtite and shonkinite (up to

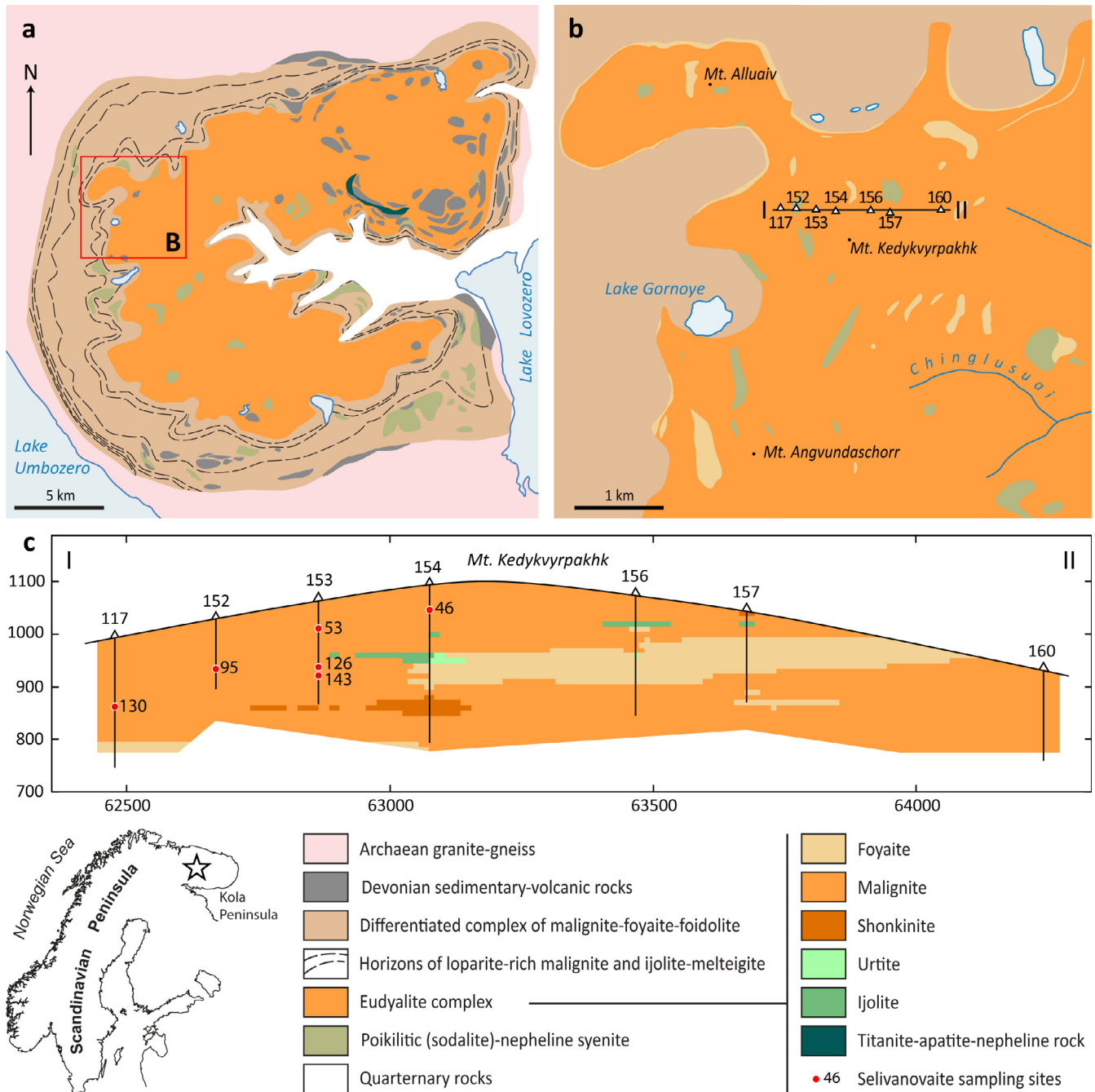


Fig. 1. Geological maps of the Lovozero alkaline massif (a, after Kalashnikov *et al.*, 2016) and Alluaiv Set of the Lovozero Loparite-Eudyalite deposit (b, after Utkin *et al.*, 1995) and its section along the I–II line with positions of selivanovaite-bearing eudyalite malignite (c).

50 m thick) as well as conformable xenoliths (up to 20 m thick) of fenitised basalts and basaltic tuffs (dark fine-grained biotite–anorthoclase rocks with relics of andesine, diopside, forsterite, ilmenite and newly formed fayalite, hercynite and cordierite–sekaninaite).

Selivanovaite was found in drill cores of medium-grained trachytoid eudyalite malignite of Mt. Kedykvyrpakhk (Fig. 2), at the horizon 850–1050 m above the Baltic Sea level (50–150 m below the present-day surface, Fig. 1c). The rock consists mainly of euhedral microcline-perthite (up to 1.5 cm in diameter), nepheline

(up to 1 cm in diameter) and (mangano)eudyalite crystals (up to 5 mm long) cemented by fine-acicular aegirine with poikilitic laths of minor lamprophyllite and selivanovaite (up to 10 modal %; on average, 3 modal %). The mean modal composition of the rock is $Kfs_{40}Nph_{30}Aeg_{20}Eud_{10}$. Other minor rock-forming minerals include sodalite, natrolite and magnesioarfvedsonite. Characteristic accessory minerals are murmanite, loparite-(Ce), pyrochlore, thorite, anatase, baryte, rhabdophane-(Ce), pyrrhotite, chalcopyrite, pyrite, chlorbarntonite, djerfisherite, sphalerite, and löllingite. The

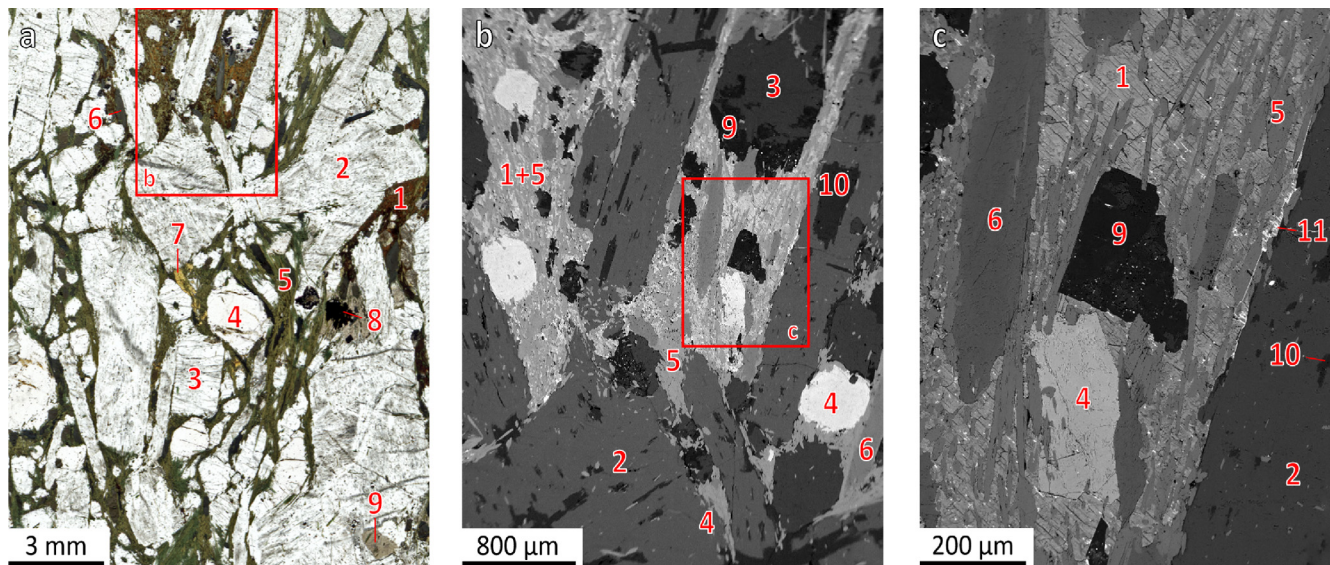


Fig. 2. Eudialyte-rich trachtyoid nepheline syenite (lujavrite) 153/126 of Mt. Kedykvyrpakhk (see Fig. 1c) with selivanovaite (1). Photo of polished thin section in transmitted light (a) and BSE-images of selected regions (b and c). Legend: 2—microcline-perthite, 3—nepheline, 4—manganoeudialyte, 5—aeirine, 6—magnesoarfvedsonite, 7—lamprophyllite, 8—pyrrhotite, pyrite, djerfisherite, chlorbartonite and löllingite, 9—natrolite, 10—albite, 11—baryte.

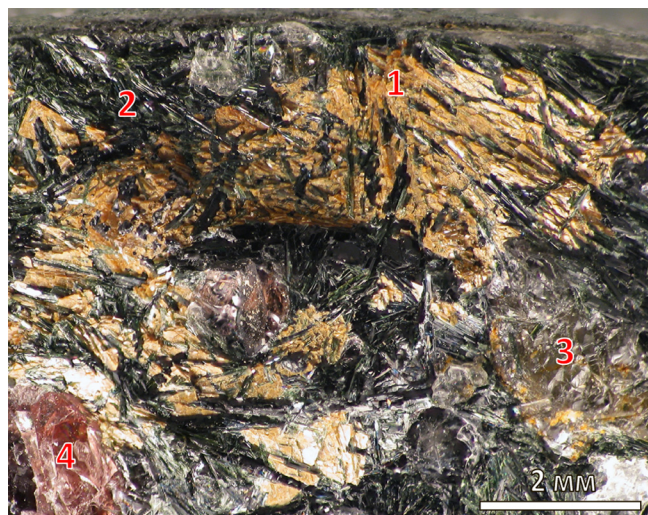


Fig. 3. Intergrowth of selivanovaite (1) and aegirine (2) in eudialyte-rich trachtyoid malignite, sample no. 117/130, Mt. Kedykvyrpakhk (see Fig. 1c). 3—nepheline, 4—manganoeudialyte.

holotype specimen of selivanovaite, no. 117/130 (Fig. 3), was studied in detail.

3. Appearance and physical properties

Selivanovaite forms platy metacrysts (up to 8 mm in diameter) flattened on (001) with numerous poikilitic inclusions of aegirine and magnesoarfvedsonite (Figs. 2 and 3). No euhedral grains have been found. The $a:b:c$ ratio calculated from the unit-cell parameters (single-crystal data) is close to 1:1:1.4. No twinning was observed. Cleavage is perfect on {001} and weak on {110}. The mineral is brittle and has a stepped fracture. Mohs

hardness is about 3. The density determined by the float-sink method in Clerici solution is $3.15(3) \text{ g} \cdot \text{cm}^{-3}$, the density calculated using the empirical formula and single-crystal unit-cell parameters is $3.34 \text{ g} \cdot \text{cm}^{-3}$. The deviation between the two values is most probably due to the inclusions of magnesoarfvedsonite.

Macroscopically, selivanovaite is dark-orange. Its lustre is vitreous to greasy on cleavage planes, and greasy to mate in cross fracture. The mineral is translucent in thin plates, with a pale brownish white streak. It is biaxial positive, with the refractive indices: $\alpha = 1.79(1)$, $\beta = 1.81(1)$, $\gamma = 1.87(1)$ (589 nm); $2V_{\text{meas}} = 40(5)^\circ$ (measured in conoscopy), $2V_{\text{calc}} = 57.3^\circ$. The optical orientation is $Z^{\wedge}c = 5\text{--}10^\circ$, other details unclear. In transmitted light selivanovaite is yellowish brown (see Fig. 2a), without pleochroism and dispersion. The mineral is non-fluorescent. A Gladstone-Dale calculation provides a compatibility index of 0.027, which is regarded as excellent.

4. Chemical composition

The chemical composition of selivanovaite was determined by wavelength-dispersive spectrometry on a Cameca MS-46 electron microprobe (Geological Institute, Kola Science Centre, Russian Academy of Sciences, Apatity) operating at 20 kV, 20–30 nA, with a 20 μm beam diameter. The standards used were: lorenzenite (Na, Ti), pyrope (Mg, Al), wollastonite (Si, Ca), wadeite (K), synthetic MnCO_3 (Mn), hematite (Fe), zircon (Zr), and synthetic LiNbO_3 (Nb). The mineral is unstable under the electron beam and loses at least part of its H_2O content after few seconds of analysis. In order to avoid the problem, the electron beam has been defocused and moved during the analyses. The H_2O content was determined by

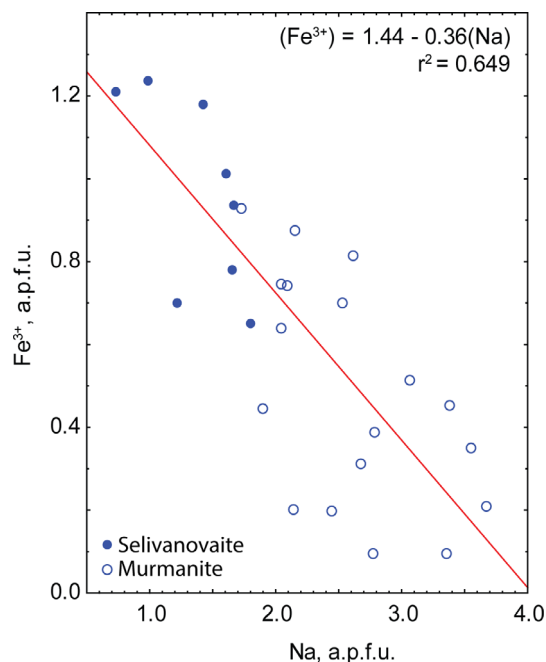


Fig. 4. Relation between the Na and Fe^{3+} contents in selivanovaite and murmanite.

the Penfield method (Sandell, 1951) on purified material of the holotype sample.

Table 1 provides mean analytical results for selivanovaite, averaged from the compositions of three crystals (each obtained as the average of 5–6 points). The empirical formula of the holotype selivanovaite (based on Si = 4 atoms per formula unit, *apfu*) can be written as $(\text{Na}_{1.65}\text{Mn}_{0.35}\text{Ca}_{0.28}\text{Zr}_{0.18}\text{Mg}_{0.14}\text{K}_{0.13})_{\Sigma 2.73}(\text{Ti}_{3.67}\text{Fe}_{0.78}^{3+}\text{Nb}_{0.47}\text{Al}_{0.01})_{\Sigma 4.93}[\text{Si}_4\text{O}_{19.72}] \cdot 8.87\text{H}_2\text{O}$. The simplified end-member formula is $\text{NaTi}_3(\text{TiNaFeMn}_{0.5}\square_{0.50})_{\Sigma 4}[(\text{Si}_2\text{O}_7)_2\text{O}_4(\text{OH})_2(\text{H}_2\text{O})_2] \cdot n\text{H}_2\text{O}$. It is noteworthy that the structure refinement (see below) indicates the H_2O content to be *ca.* 1.72 *pfu*, which implies the presence of a significant amount of non-structural (adsorbed) water (up to 7 H_2O *pfu*). Similar to murmanite, the non-structural H_2O can be eliminated easily in vacuum or under even mild heating.

There are no clear relations between different cation contents in selivanovaite, but the comparison with co-existing murmanite indicates the increase of the Fe content at the expense of Ti and especially Na (Fig. 4) due to the isomorphic substitutions $2\text{Na}^+ + \text{Ti}^{4+} \leftrightarrow \square + 2\text{Fe}^{3+}$ and/or $\text{Na}^+ + \text{Ti}^{4+} \leftrightarrow \text{Ca}^{2+} + \text{Fe}^{3+}$.

Selivanovaite dissolves slowly in 10% cold HCl.

5. Raman spectroscopy

The Raman spectrum of selivanovaite (Fig. 5) was obtained using a Horiba Jobin-Yvon LabRam HR 800 spectrometer (“Geomodel” Resource Centre of St. Petersburg State University). The mineral is very unstable under the laser beam.

The spectrum shows eleven vibrational bands that can be assigned to symmetric bending vibrations of H_2O molecules at 1600 cm^{-1} , symmetric and antisymmetric

bending vibrations of SiO_4 groups in the region between 690 and 434 cm^{-1} . Bands at 780 , 930 cm^{-1} can be interpreted as different modes of Si–O stretching vibrations. The bands at 610 , 281 , 180 cm^{-1} correspond to the symmetric stretching and bending vibrations of the TiO_6 , FeO_6 and MgO_6 groups. The bands at 77 , 104 , 147 cm^{-1} can be assigned to lattice vibrations.

6. Powder X-ray diffraction

The powder X-ray diffraction pattern of selivanovaite (Table 2) was measured from a powder microsample using a Rigaku R-AXIS RAPID II diffractometer equipped with a cylindrical image plate detector using Debye-Scherrer geometry ($d = 127.4\text{ mm}$; $\text{CoK}\alpha$ radiation). The data were integrated using the software package *OSC2XRD* (Britvin *et al.*, 2017). Unit-cell parameters determined from powder patterns are: $a = 8.673(5)$, $b = 8.694(1)$, $c = 12.21(1)\text{ \AA}$, $\alpha = 92.70(5)$, $\beta = 108.52(1)$, $\gamma = 105.42(1)^\circ$, $V = 833(1)\text{ \AA}^3$ and $Z = 2$, which are in good agreement with the single-crystal data. The strongest X-ray powder-diffraction lines [listed as d in Å (J) (hkl)] are: $11.43(1\ 0\ 0)$ ($0\ 0\ 1$), $6.37(25)(-1\ 1\ 1)$, $5.73(15)(0\ 0\ 2)$, $4.208(16)(-2\ 1\ 1)$, $3.108(35)(2\ -2\ 1)$, $3.043(20)(-1\ 0\ 4)$, and $2.596(17)(0\ 1\ 4)$.

7. Crystal structure

7.1. Experimental procedure

Single-crystal X-ray diffraction analysis was performed by means of an Agilent Technologies SuperNova diffractometer ($\text{MoK}\alpha$ radiation; $\lambda = 0.71069\text{ \AA}$) equipped with the $\text{I}\mu\text{S}$ microfocus X-ray source and a CCD area detector operated at 50 kV and 0.8 mA . A hemisphere of three-dimensional data was collected with frame widths of 1° in ω , and a 650 s exposure in the 2θ range $6.40\text{--}50^\circ$ (the time of experiment was nearly 72 h). Due to the small size ($0.015 \times 0.015 \times 0.002\text{ mm}^3$), extremely weak diffraction (co-existing murmanite with the same size shows more than 10 times brighter reflections) and low quality of the crystals (Fig. 2b), the quality of the structure refinement was far from being perfect. For these reasons, the final structural model is of a relatively low quality. The data were integrated and corrected by means of the *CrysAlisPro* (Agilent Technologies, 2014) program package, which was also used to apply empirical absorption correction using spherical harmonics, implemented in the *SCALE3* *ABSPACK* scaling algorithm. The basic features of crystal structure were determined via *SHELX* program package (Sheldrick, 2008) and refined to $R_1 = 0.193$ ($R_{\text{int}} = 0.165$) for 2881 independent reflections with $F_o > 4\sigma(F_o)$ in the $P\bar{1}$ space group. Occupancies of the cation sites were calculated from the experimental site-scattering factors (except low-occupancy sites) in accordance with the empirical chemical composition. Hydrogen sites could not be located. Atom labels are given according to the current classification of the seidozerite-supergroup minerals

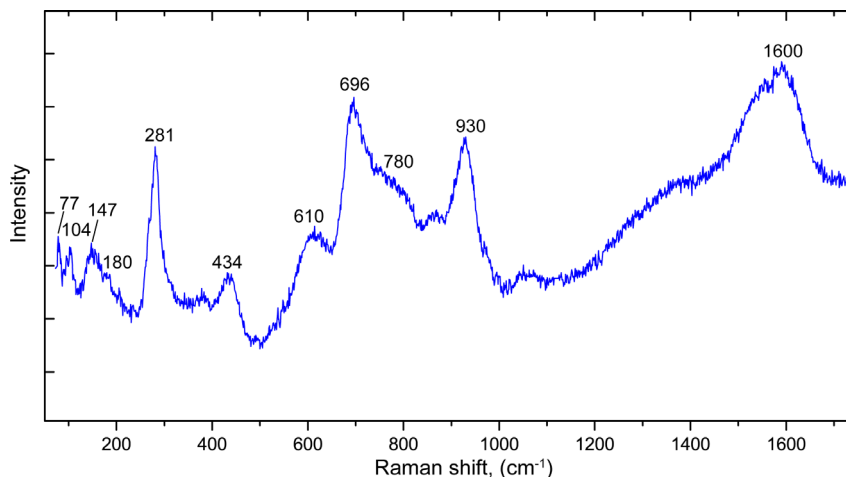


Fig. 5. Raman spectrum of selivanovaite.

Table 2. X-ray powder-diffraction data for selivanovaite (strongest lines in bold-face type).

I_{meas}	$d_{\text{meas}}, \text{\AA}$	I_{calc}	$d_{\text{calc}}, \text{\AA}$	hkl
100	11.43	100	11.46	0 0 1
25	6.37	9	6.37	$\bar{1}$ 1 1
15	5.73	34	5.73	0 0 2
7	4.440	2	4.427	0 1 2
16	4.208	19	4.203	2 1 1
13	4.102	15	4.088	0 2 1
4	3.904	4	3.909	1 2 1
5	3.191	6	3.200	2 1 0
35	3.108	8	3.109	2 2 1
20	3.043	3	3.050	$\bar{1}$ 0 4
11	2.990	2	2.996	2 $\bar{1}$ 3
8	2.905	2	2.898	$\bar{1}$ $\bar{1}$ 4
17	2.596	15	2.596	0 1 4
6	2.532	7	2.533	0 2 4
14	2.496	10	2.495	3 $\bar{1}$ 1
5	2.225	4	2.224	1 2 3
3	2.107	2	2.108	2 4 0
2	2.103	2	2.102	4 2 2
4	1.8781	4	1.8790	1 1 5
6	1.7944	7	1.7947	4 1 0
5	1.7383	3	1.7375	2 0 5
4	1.6980	4	1.6975	3 2 2
3	1.6363	3	1.6366	3 5 0
3	1.5697	2	1.5698	$\bar{2}$ 5 3
5	1.5541	7	1.5542	3 2 3
4	1.5259	3	1.5258	$\bar{3}$ $\bar{2}$ 7
2	1.5060	2	1.5059	4 5 2
4	1.4252	3	1.4249	4 $\bar{3}$ 5

(Sokolova & Cámara, 2017). Crystal data, data-collection information and structure-refinement details are given in Table 3, atom coordinates and selected interatomic distances are in Tables 4 and 5, respectively. Anisotropic displacement parameters and other details of structure refinement are deposited as a supplementary CIF (Crystallographic Information File), linked to this article and freely available at <https://pubs.geoscienceworld.org/eurjmin>.

Table 3. Single-crystal data and refinement parameters for selivanovaite.

Temperature/K	293(2)
Crystal system	Triclinic
Space group	$P\bar{1}$
a (Å)	8.673(5)
b (Å)	8.694(3)
c (Å)	12.213(14)
α (°)	92.70(5)
β (°)	108.46(7)
γ (°)	105.40(4)
Volume (Å ³)	833.4(12)
Z	2
ρ_{calc} (g/cm ³)	3.183
μ (mm ⁻¹)	3.273
$F(000)$	771.0
Crystal size (mm ³)	0.015 × 0.015 × 0.002
Radiation	MoK α ($\lambda = 0.71073$)
2 θ range for data collection/°	6.402 to 49.998
Index ranges	$-10 \leq h \leq 10$, $-10 \leq k \leq 10$, $-14 \leq l \leq 14$
Reflections collected	5962
Independent reflections	2902 [$R_{\text{int}} = 0.1651$, $R_{\text{sigma}} = 0.2716$]
Data/restraints/parameters	2902/42/201
Goodness-of-fit on F^2	1.150
Final R indices [$I \geq 2\sigma I$]	$R_1 = 0.1937$, $wR_2 = 0.4150$
Final R indices [all data]	$R_1 = 0.3092$, $wR_2 = 0.5121$
Largest diff. peak/hole (e^-)	3.60/−1.85

7.2. Structure description

The crystal structure of selivanovaite is based on TS block (Sokolova & Cámara, 2017) or HOH modules (Ferraris, 1997) consisting of two types of layers parallel to (0 0 1) (Fig. 6) interlinked by I -block cations like in other murmanite- and lamprophyllite-group minerals (Guan *et al.*, 1963; Chernov *et al.*, 1971; Sokolova & Cámara, 2017). Though the selivanovaite structure belongs to a new structure type of minerals and inorganic compounds,

Table 4. Atom coordinates, isotropic displacement parameters (\AA^2) and site occupancies for the crystal structure of selivanovaite.

Site	Occupancy	x	y	z	U_{eq}
$A^{\text{P}}1$	Na _{0.50}	0.202(3)	0.778(2)	-0.0016(18)	0.018(5)
$M^{\text{H}}1$	Ti	0.0826(7)	0.8126(6)	0.2226(5)	0.0191(15)
$M^{\text{H}}2$	Ti _{0.74(3)} Zr _{0.26(3)}	0.3136(6)	0.5803(6)	0.2177(5)	0.039(2)
$M^{\text{H}}3$	Ti _{0.64(3)} Nb _{0.36(3)}	0.1447(7)	0.9492(6)	-0.2270(6)	0.052(3)
$M^{\text{O}}1$	Ti _{0.79(3)} Nb _{0.21(3)}	0.0607(6)	0.6983(5)	0.5065(5)	0.034(2)
$M^{\text{O}}2$	Fe _{0.62(11)} Ti _{0.38(11)}	0.5864(7)	0.1947(5)	0.5110(5)	0.031(2)
$M^{\text{O}}3$	Na	0.8165(16)	0.9300(15)	0.5056(11)	0.029(3)
$M^{\text{O}}4$	Mn _{0.20} Na _{0.18} Ca _{0.12}	0.349(3)	0.4481(19)	0.5065(17)	0.055(8)
Si1	Si	-0.0580(11)	0.4471(10)	0.2558(9)	0.027(2)
Si2	Si	0.4731(12)	0.9765(10)	0.2595(9)	0.033(3)
Si3	Si	-0.2617(11)	0.6622(9)	0.2727(10)	0.032(3)
Si4	Si	0.7214(12)	0.8024(10)	0.7245(9)	0.029(2)
O1	O	0.070(3)	0.575(3)	0.2141(19)	0.035(6)
O2	O	-0.237(3)	0.497(3)	0.2147(19)	0.038(6)
O3	O	0.014(3)	0.469(3)	0.3987(19)	0.030(5)
O4	O	-0.110(3)	0.271(3)	0.1967(19)	0.035(6)
O5	O	0.622(3)	0.994(3)	0.2134(18)	0.033(5)
O6	O	0.598(4)	0.865(3)	0.777(2)	0.048(7)
O7	O	0.528(3)	0.980(3)	0.4055(19)	0.031(5)
O8	O	0.323(3)	0.822(2)	0.2093(18)	0.029(5)
O9	O	0.822(2)	0.691(2)	0.4118(16)	0.016(4)
O10	O	-0.154(3)	0.810(3)	0.221(2)	0.039(6)
O11	O	-0.465(3)	0.635(3)	0.2199(19)	0.035(6)
O12	O	0.642(3)	0.777(3)	0.5849(19)	0.034(6)
O13	O	0.736(3)	0.644(3)	0.778(2)	0.046(7)
O14	O	0.889(3)	0.938(3)	0.768(2)	0.046(7)
$X^{\text{O}}_{\text{A}1}$	O	0.391(3)	0.632(2)	0.3829(18)	0.030(5)
$X^{\text{O}}_{\text{A}2}$	O	0.287(3)	0.688(3)	0.5731(19)	0.036(6)
$X^{\text{O}}_{\text{M}1}$	O	0.075(3)	0.880(2)	0.6138(18)	0.029(5)
$X^{\text{O}}_{\text{M}2}$	O	0.829(3)	0.182(3)	0.5966(19)	0.031(5)
$X^{\text{H}}_{\text{A}1}$	H ₂ O	0.463(4)	0.758(4)	-0.049(3)	0.070*
$X^{\text{H}}_{\text{A}2}$	(OH) _{0.76} (H ₂ O) _{0.24}	-0.011(4)	0.781(3)	0.042(2)	0.059(8)
$X^{\text{H}}_{\text{M}1}$	(OH) _{0.76} (H ₂ O) _{0.24}	0.226(4)	0.547(3)	0.042(2)	0.062(8)
$X^{\text{H}}_{\text{M}2}$	(OH) _{0.76} (H ₂ O) _{0.24}	0.217(3)	1.001(3)	-0.0456(18)	0.033(5)

* Fixed during refinement.

vigrishinite (Pekov *et al.*, 2012) is closely related to selivanovaite, but differs in geometry and stereochemistry of the *H*-sheets.

The *H*-sheets (tetrahedral-octahedral layers) consist of chains of trimers of $M^{\text{H}}1$ - $M^{\text{H}}2$ - $M^{\text{H}}3$ octahedra sharing corners with two Si_2O_7 groups (Fig. 6a). All $M^{\text{H}}1,2,3$ sites are predominantly occupied by Ti with admixtures of Nb, Fe and Zr: the refined occupancies are $^{\text{H}}1(\text{Ti}_{1.00})$, $^{\text{H}}2(\text{Ti}_{0.74}\text{Zr}_{0.26})_{1.00}$ and $^{\text{H}}3(\text{Ti}_{0.64}\text{Nb}_{0.36})$, which in good agreement with the corresponding $\langle M^{\text{H}}-\text{O} \rangle$ distances of 2.08, 1.97 and 2.00 Å, respectively. In contrast to murmanite, the crystal structure of selivanovaite contains two non-equivalent Si_2O_7 groups (Fig. 6c). Compared to murmanite, one half of the Na-sites is replaced by Ti-octahedra in selivanovaite, whereas the second half is vacant. This difference results in different geometries of the two Si_2O_7 groups in selivanovaite as shown in Fig. 7. The $\angle \text{O}-\text{O}-\text{O}$ internal angle associated with the $M^{\text{H}}1$ site is 78°, whereas the angle associated with vacancy is 158°. The same type of *H*-sheets was observed in 'murmanite' described by Rastsvetaeva & Andrianov (1986), for which, unfortunately, the chemical composition has not been reported. However, all other structural refinements of

murmanite (Khalilov *et al.*, 1965; Khalilov, 1989; Cámara *et al.*, 2008) reported the presence of the *H*-sheet of the type shown in Fig. 6c. Therefore, it is very likely that the 'murmanite' studied by Rastsvetaeva & Andrianov (1986) could in fact be selivanovaite.

The octahedral *O*-sheet is based on parallel zig-zag chains running along [1 0 0] direction and consisting of face-sharing $M^{\text{O}}1$ - $M^{\text{O}}2$ octahedra occupied by Ti and Fe (Fig. 6b). The refined occupancies of the $M^{\text{O}}1$ and $M^{\text{O}}2$ sites are $(\text{Ti}_{0.79}\text{Nb}_{0.21})_{1.00}$ and $(\text{Fe}_{0.62}\text{Ti}_{0.38})_{1.00}$, respectively, and the mean $\langle M^{\text{O}1,2}-\text{O} \rangle$ distances are 2.01 and 2.00 Å, respectively. The $M^{\text{O}}3$ - $M^{\text{O}}4$ octahedral chains fill interstices between the $M^{\text{O}}1$ - $M^{\text{O}}2$ octahedral chains. The $M^{\text{O}}4\text{O}_6$ octahedron is more distorted than the $M^{\text{O}}3\text{O}_6$ octahedron and is half-occupied only, due to the short $M^{\text{O}}4$ - $M^{\text{O}}4$ distance of 2.60 Å. The refined occupancies of the $M^{\text{O}}3$ and $M^{\text{O}}4$ sites are $(\text{Na})_{1.00}$ and $(\text{Mn}_{0.20}\text{Na}_{0.18}\text{Ca}_{0.12})_{\Sigma 0.50}$ respectively (the occupancy of the $M^{\text{O}}4$ site containing three elements was re-calculated using average site-scattering factor), and the mean $\langle M^{\text{O}3,4}-\text{O} \rangle$ distances are 2.39 and 2.43 Å, respectively. In general, the *O*-sheet in selivanovaite can be considered as slightly modified *O*-sheet in murmanite.

Table 5. Selected interatomic distances (Å) in the crystal structure of selivanovaite

A^P1-O4	2.24(3)	$M^{H3}-X^P_{M2}$	2.09(2)	M^P4-O12	2.24(3)
A^P1-O8	2.42(3)	$\langle M^{H3}-O \rangle$	2.00	$M^P4-X^P_{A1}$	2.53(3)
$A^P1-X^P_{A1}$	2.55(4)			$M^P4-X^P_{A1}$	2.29(3)
$A^P1-X^P_{A2}$	2.08(4)	M^P1-O3	2.00(2)	$M^P4-X^P_{A2}$	2.46(3)
$A^P1-X^P_{M1}$	2.15(3)	M^P1-O3	2.20(2)	$\langle M^P4-O \rangle$	2.43
$A^P1-X^P_{M2}$	2.02(3)	M^P1-O9	2.01(2)		
$\langle A^P1-O \rangle$	2.24	$M^P1-X^P_{A2}$	1.90(2)	Si1-O1	1.58(3)
		$M^P1-X^P_{M1}$	1.95(2)	Si1-O2	1.65(2)
$M^{H1}-O1$	2.03(2)	$M^P1-X^P_{M2}$	1.99(2)	Si1-O3	1.64(2)
$M^{H1}-O8$	2.13(2)	$\langle M^P1-O \rangle$	2.01	Si1-O4	1.55(2)
$M^{H1}-O10$	2.04(3)			$\langle Si1-O \rangle$	1.61
$M^{H1}-O14$	2.11(2)	M^P2-O7	2.08(2)		
$M^{H1}-X^P_{M2}$	2.09(2)	M^P2-O7	2.06(2)	Si2-O5	1.54(2)
$M^{H1}-X^P_{A2}$	2.07(3)	M^P2-O12	2.04(2)	Si2-O6	1.68(3)
$\langle M^{H1}-O \rangle$	2.08	$M^P2-X^P_{A1}$	1.87(2)	Si2-O7	1.69(2)
		$M^P2-X^P_{A2}$	1.88(2)	Si2-O8	1.53(2)
$M^{H2}-O1$	2.09(2)	$M^P2-X^P_{M2}$	2.07(2)	$\langle Si2-O \rangle$	1.61
$M^{H2}-O8$	2.09(2)	$\langle M^P2-O \rangle$	2.00		
$M^{H2}-O11$	1.85(2)			Si3-O2	1.67(2)
$M^{H2}-O13$	1.89(2)	M^P3-O7	2.58(2)	Si3-O9	1.60(2)
$M^{H2}-X^P_{A1}$	1.90(2)	M^P3-O9	2.34(2)	Si3-O10	1.66(3)
$M^{H2}-X^P_{M1}$	2.01(3)	M^P3-O12	2.23(3)	Si3-O11	1.62(2)
$\langle M^{H2}-O \rangle$	1.97	$M^P3-X^P_{M1}$	2.45(3)	$\langle Si3-O \rangle$	1.64
		$M^P3-X^P_{M2}$	2.38(2)		
$M^{H3}-O4$	1.93(2)	$M^P3-X^P_{M2}$	2.37(2)	Si4-O6	1.60(3)
$M^{H3}-O5$	1.90(2)	$\langle M^P3-O \rangle$	2.39	Si4-O12	1.60(2)
$M^{H3}-O10$	2.07(2)			Si4-O13	1.57(3)
$M^{H3}-O14$	2.17(3)	M^P4-O3	2.85(3)	Si4-O14	1.52(3)
$M^{H3}-X^P_{M1}$	1.86(2)	M^P4-O9	2.18(3)	$\langle Si4-O \rangle$	1.57

The *HOH* layers (Fig. 8) are connected by the Na-occupied A^P1O_6 octahedra, which, according to Sokolova & Cámara (2017) are assigned to the *I*-block group sites. The A^P1 site has the scattering factor of 5.5 *e* and the mean $\langle A^P-O \rangle$ distance of 2.24 Å, which agrees well with the (Na)_{0.50} occupancy.

The crystal-chemical formula of selivanovaite is ${}^A(Na_{0.50}, \square_{0.50})_{\Sigma 1.00} {}^H(Ti_{2.38}Nb_{0.36}Zr_{0.26})_{\Sigma 3.00} {}^M(Ti_{1.17}Na_{1.18}Fe_{0.62}\square_{0.50}Mn_{0.20}Ca_{0.12}Nb_{0.21})_{\Sigma 4.00}(Si_2O_7)_2^{XO}\{O_4\}^{XP}\{(OH)_{2.28}(H_2O)_{1.72}\}$, which is in a good agreement with the empirical formula. The difference between the H₂O contents in structural and empirical formulas (1.72 and 7 *apfu*, respectively) of the holotype selivanovaite is due to the presence of additional non-structural H₂O molecules within interlayers (which is also a specific feature of murmanite). The idealized end-member formula of selivanovaite can be written as $NaTi_3(TiNaFeMn_{0.5}\square_{0.50})_{\Sigma 4}[(Si_2O_7)_2O_4(OH)_2(H_2O)_2]$ without non-structural H₂O and $NaTi_3(TiNaFeMn_{0.5}\square_{0.50})_{\Sigma 4}[(Si_2O_7)_2O_4(OH)_2(H_2O)_2] \cdot nH_2O$ with non-structural H₂O, where, for the holotype sample, $n \sim 5$.

Indeed, the H₂O content in murmanite of the Lovozero massif ranges from 6 to 11 *apfu*, and its very simplified formula can be written as $Na_4Ti_4Si_4O_{18} \cdot nH_2O$ (Vlasov *et al.*, 1966; Khomyakov, 1995; Pekov, 2000; Németh *et al.*, 2005). However, this mineral contains only 4 structural H₂O molecules *pfu*, while most of the H₂O is non-structural and can be removed from the mineral by

heating up to 200 °C (Vlasov *et al.*, 1966). Similarly, the H₂O content in selivanovaite ranges from 2 to 8 H₂O *pfu*, but only 2 H₂O *pfu* are detected by the crystal-structure analysis. Thus, by analogy to murmanite, the real composition of selivanovaite corresponds to the formula $NaTi_3(Ti,Na,Fe,Mn)_4[(Si_2O_7)_2O_4(OH,H_2O)_4] \cdot nH_2O$.

8. Discussion

According to Sokolova & Cámara (2017), the murmanite group contains seidozerite-supergrupp minerals with Ti (+ Nb + Fe³⁺ + Zr + Mn + Mg) = 4 *apfu*. Technically speaking, the corresponding sum in selivanovaite is equal to 5.59 and 5.00 *apfu* according to the chemical analysis and the crystal-structure refinement, respectively. Such a situation is not foreseen in the nomenclature scheme suggested by Sokolova & Cámara (2017) and, tentatively, we assign selivanovaite to the murmanite group as the closest one according to the crystal-chemical considerations.

There are two possible scenarios for the genesis of selivanovaite. In the first scenario, selivanovaite and murmanite are considered as mineral species that form independently from each other, which is supported by the fact that crystals of these minerals commonly co-exist in one sample without any reaction relations between them.

According to the second scenario proposed by analogy with calciomurmanite, vigrishinite and zvyaginite, selivanovaite can be considered as a murmanite-derived mineral, via the $Na^+ + Ti^{4+} \rightarrow Ca^{2+} + Fe^{3+}$ cation exchange and the re-organization of *H*-layers of *HOH*-pockets (Fig. 8). This transition is accompanied by the transformation of the unit-cell size from (5.4 × 7.1 × 12.1 Å) to (8.7 × 8.7 × 12.0 Å), which has also been reported for the murmanite–vigrishinite series (Lykova *et al.*, 2016).

During this transformation, one half of Na positions within the *H*-layer of murmanite is replaced by Ti and Fe³⁺, whereas the second one becomes vacant. As a result, respective [Si₂O₇] groups experience different distortions and the unit-cell changes, resulting in the formation of a supercell. At the same time the epistolite → zvyaginite transition (with the same change in the unit-cell dimensions) occurs due to the cation ordering in the *O*-sheet (Sokolova & Cámara, 2017; Sokolova *et al.*, 2017). It seems that selivanovaite combines both mechanisms: both *H*- and *O*-sheets of selivanovaite show significant differences in their topology from those of murmanite. It is noteworthy that the same difference of topology of the *H*-sheets is characteristic for the epistolite–zvyaginite pair (Pekov *et al.*, 2014).

Within the Lovozero eudialyte complex, the highest contents of Ca, Fe and Ti are characteristic for basalt xenoliths located within the alkaline-rock layers (Korchak *et al.*, 2011). Fenitization of basalt and its tuff, sufficiently enriched in magnetite–ulvöspinel, ilmenite and rutile, produces a Ca–Fe–Ti-rich fluid that causes metasomatic alteration of surrounding alkaline rocks and transforma-

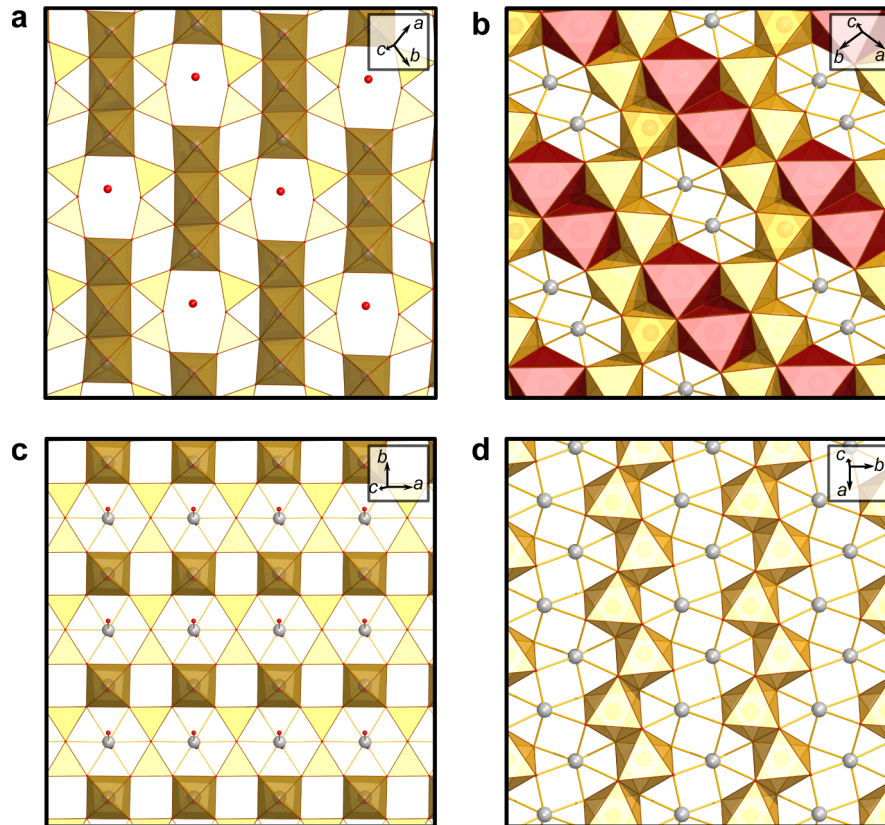


Fig. 6. Heteropolyhedral (*H*) (a) and octahedral (*O*) sheets (b) in the crystal structure of selivanovaite and the *H*- (c) and *O*-sheets (d) in murmanite. Half-occupied M^4 and A^1 sites are shown as grey spheres, SiO_4 tetrahedra are highlighted in yellow, the M^{H1} , M^{H2} , M^{H3} octahedra are pale brown, the M^1 , M^2 octahedra are orange, the M^3 octahedra are red.

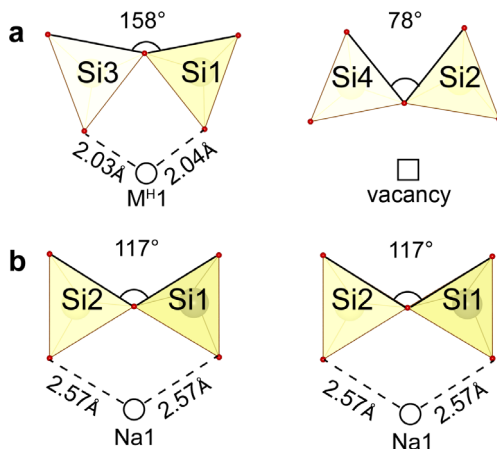
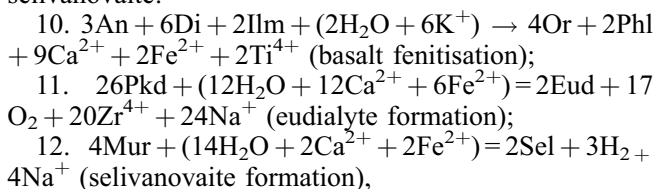


Fig. 7. Configurations of the Si_2O_7 groups in the crystal structure of selivanovaite (a) and murmanite (b).

tion of primary parakeldyshite into manganoendialyte (Ivanyuk *et al.*, 2015) and primary murmanite into selivanovaite:



where An – anorthite; Di – diopside; Eud – eudialyte, $\text{Na}_{14}\text{Ca}_6\text{Fe}_3\text{Zr}_3\text{Si}_{26}\text{O}_{72}(\text{OH})_4 \cdot 4\text{H}_2\text{O}$; Ilm – ilmenite; Mur – murmanite, $\text{Na}_4\text{Ti}_4\text{Si}_4\text{O}_{18} \cdot 4\text{H}_2\text{O}$; Pkd – parakeldyshite, $\text{Na}_2\text{ZrSi}_2\text{O}_7$; Or – orthoclase; Phl – phlogopite; Sel – selivanovaite, $\text{Na}_2\text{CaFeTi}_4\text{Si}_4\text{O}_{17}(\text{OH})_5 \cdot 7\text{H}_2\text{O}$.

Following this scheme, selivanovaite spreads in those regions of eudialyte malignite layers, where murmanite contains sufficient amounts of Ca and Fe at the expense of Na and Ti. Manganese content in eudialyte malignite gradually increases with depth, which causes in turn transition of eudialyte into manganoendialyte and enrichment of selivanovaite in Mn instead of Fe. Therefore, selivanovaite most likely crystallizes as a transition mineral formed together with eudialyte during alteration of primary murmanite and parakeldyshite by the Ca–Fe–Ti-rich fluid originated from metasomatic alteration of basalt xenoliths by alkaline melt.

Acknowledgements: It is our pleasure to dedicate this work to Giovanni Ferraris and Stefano Merlino, who made profound contributions to various fields of mineralogical crystallography and, in particular, to our understanding of the role of modularity in minerals. We also appreciate very much their collaboration with Russian mineralogists, especially in the difficult times of the 1990s. We are grateful to Joel Grice, an anonymous reviewer and Christian Chopin for the useful comments on the

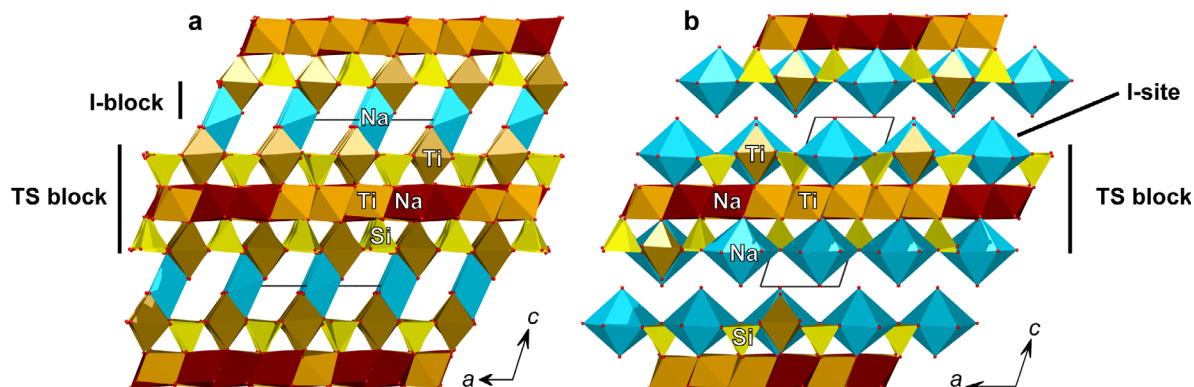


Fig. 8. The crystal structures of selivanovaitite (a) and murmanite (b) projected along the direction parallel to the TS blocks. The coordination polyhedra of the *I* site are shown light blue; other legend as in Fig. 6.

manuscript. This research was supported by the Presidium of Russian Academy of Sciences, program 4 (field works in 2015–2016, sampling, study of rock-forming minerals), and the Russian Science Foundation, grant 16-17-10173 (3D mapping of the Lovozero eudialyte complex and the selivanovaitite investigation).

References

- Agilent Technologies (2014): CrysAlis CCD and CrysAlis RED. Oxford Diffraction Ltd, Yarnton, Oxfordshire, UK.
- Belov, N.V. & Organova, N.I. (1962): Crystal chemistry and mineralogy of the lomonosovite group in the light of the crystal structure of lomonosovite. *Geokhimiya*, **1**, 4–13 (in Russian).
- Britvin, S.N., Dolivo-Dobrovolsky, D.V., Krzhizhanovskaya, M.G. (2017): Software for processing of X-ray powder diffraction data obtained from the curved image plate detector of Rigaku RAXIS Rapid II diffractometer. *Zap. Ross. Mineral. Obsh.*, **146**, 104–107
- Bussen, I.V. & Sakharov, A.S. (1972): Petrology of the Lovozero Alkaline Massif. Nauka, Leningrad, 296 (in Russian).
- Cámara, F., Sokolova, E., Hawthorne, F. C., Abdu, Y. (2008): From structure topology to chemical composition. IX. Titanium silicates: revision of the crystal chemistry of lomonosovite and murmanite, Group-IV minerals. *Mineral. Mag.*, **72**, 1207–1228.
- Chernov, A.N., Ilyukhin, V.V., Maksimov, B.A., Belov, N.V. (1971): Crystal structure of inelilite, $\text{Na}_2\text{Ba}_3(\text{Ba},\text{K},\text{Mn})(\text{Ca},\text{Na})\text{Ti}(\text{TiO}_2)_2[\text{Si}_2\text{O}_7]_2(\text{SO}_4)_2$. *Sov. Phys. Crystallogr.*, **16**, 65–69.
- Egorov-Tismenko, Yu.K. & Sokolova, E.V. (1987): Comparative crystal chemistry of a group of titanium silicate analogues of mica. in “Comparative Crystal Chemistry”. Moscow State University, Moscow, 96–106 (in Russian).
- , — (1990): Homologous series seidozerite-nacaphite. *Mineral. Zh.*, **12**, 40–49 (in Russian).
- Ferraris, G. (1997): Polysomatism as a tool for correlating properties and structure. in “Modular Aspects of Minerals” S. Merlino ed., Eötvös University Press, Budapest, 275–295.
- Ferraris, G. (2006): Pillared materials from layer titanositates? *Solid St. Phenom.*, **111**, 47–50.
- (2008a): Modular structures – the paradigmatic case of heterophyllosilicates. *Z. Kristallogr.*, **223**, 76–84.
- Ferraris, G. (2008b): Heterophyllosilicates, a potential source of nanolayers for materials science. in “Minerals as Advanced Materials I”. S.V. Krivovichev ed., Springer, 157–163.
- Ferraris, G., Ivaldi, G., Khomyakov, A.P., Soboleva, S.V., Belluso, E., Pavese, A. (1996): Nafertisite, a layer titanositate member of a polysomatic series including mica. *Eur. J. Mineral.*, **8**, 241–249.
- Ferraris, G., Makovicky, E., Merlino S. (2004): Crystallography of Modular Materials. Oxford University Press, Oxford, 370
- Ferraris, G., Bloise, A., Cadoni, M. (2008): Layered titanositates – A review and some results on the hydrothermal synthesis of bafertisite. *Micropor. Mesopor. Mater.*, **107**, 108–112.
- Gerasimovsky, V.I., Volkov, V.P., Kogarko, L.N., Polyakov, A.I., Saprykina, T.V., Balashov Yu.A. (1966): Geochemistry of the Lovozero Alkaline Massif. Nauka, Moscow, 396 (in Russian).
- Guan, Ya.S., Simonov, V.I., Belov, N.V. (1963): Crystal structure of bafertisite, $\text{BaFe}_2\text{TiO}[\text{Si}_2\text{O}_7](\text{OH})_2$. *Dokl. AN SSSR*, **149**, 123–126 (in Russian).
- Ivanyuk, G.Yu., Pakhomovsky, Ya.A., Yakovenchuk, V.N. (2015): Eudialyte-group minerals in rocks of Lovozero layered complex at Mt. Karnasurt and Mt. Kedykvyrpakhk. *Geol. Ore Dep.*, **57**, 600–613.
- Kalashnikov, A.O., Konopleva, N.G., Pakhomovsky, Ya.A., Ivanyuk, G. Yu. (2016): Rare earth deposits of the Murmansk region, Russia—a review. *Econ. Geol.*, **111**, 1529–1559.
- Khalilov, A.D. (1989): Refinement of the crystal structure of murmanite and new data on its crystal-chemical characteristics. *Mineral. Zh.*, **11**, 19–27 (in Russian).
- Khalilov, A.D., Mamedov, K.S., Makarov, E.S., Pyanzina, L.A. (1965): Crystal structure of murmanite. *Dokl. AN SSSR*, **161**, 1409–1411 (in Russian).
- Khomyakov, A.P. (1995): Mineralogy of Hyperagpaitic Alkaline Rocks. Clarendon Press, Oxford, USA, 223.
- Korchak, Yu.A., Men’shikov, Yu.P., Pakhomovskii, Ya.A., Yakovenchuk, V.N., Ivanyuk, G.Yu. (2011): Trap formation of the Kola Peninsula. *Petrol.*, **19**, 87–101.
- Lykova, I.S. (2015): Minerals of epistolite group: its post-crystallization changes mechanisms (natural systems and model experiments). PhD thesis. Moscow (in Russian).
- Lykova, I.S., Pekov, I.V., Chukanov, N.V., Belakovskiy, D.I., Yapaskurt, V.O., Zubkova, N.V., Britvin, S.N., Giester, G. (2016): Calciomurmanite, $(\text{Na},\square)_2\text{Ca}(\text{Ti},\text{Mg},\text{Nb})_4[\text{Si}_2\text{O}_7]_2\text{O}_2(\text{OH},\text{O})_2(\text{H}_2\text{O})_4$, a new mineral from the Lovozero and Khibiny alkaline complexes, Kola Peninsula, Russia. *Eur. J. Mineral.*, **28**, 835–845.
- Németh, P., Ferraris, G., Radnóczy, G., Ageeva, O.A. (2005): TEM and X-ray study of syntactic intergrowths of epistolite, murmanite and shkatulkalite. *Can. Mineral.*, **43**, 973–987.

- Pakhomovsky, Ya.A., Ivanyuk, G.Yu., Yakovenchuk, V.N. (2014): Loparite-(Ce) in rocks of the Lovozero layered complex at Mt. Karnasurt and Mt. Kedykvyrpakhk. *Geol. Ore Dep.*, **56**, 685–698.
- Pekov, I.V. (2000): Lovozero Massif: History, Pegmatites, Minerals. Ocean Pictures Ltd., Moscow, 480.
- Pekov, I.V., Britvin, S.N., Zubkova, N.V., Chukanov, N.V., Bryzgalov, I.A., Lykova, I.S., Belakovskiy, D.I., Pushcharovskiy, D.Yu. (2012): Vigrishinite, $Zn_2Ti_{4-x}Si_4O_{14}(OH, H_2O, \square)_8$, a new mineral from Lovozero alkaline massif (Kola Peninsula, Russia). *Zap. Ross. Mineral. Obshch.*, **141**, 12–27 (in Russian).
- Pekov, I.V., Lykova, I.S., Chukanov, N.V., Yapaskurt, V.O., Belakovskiy, D.I., Zolotarev, A.A., Zubkova, N.V. (2014): Zvyaginite, $NaZnNb_2Ti[Si_2O_7]_2O(OH,F)_3(H_2O)_{4+x}$ ($x < 1$), a new mineral of the epistolite group from the Lovozero Alkaline Pluton, Kola Peninsula, Russia. *Geol. Ore Dep.*, **56**, 644–656.
- Rastsvetaeva, R.K. & Andrianov, V.I. (1986): New data on the crystal structure of murmanite. *Sov. Phys. Crystallogr.*, **31**, 44–48.
- Sandell, E.B. (1951): Micro determination of water by the Penfield method. *Microchim. Acta*, **38**, 487–491.
- Selivanova, E.A., Yakovenchuk, V.N., Pakhomovsky, Ya.A., Ivanyuk, G. Yu. (2008): Features of low-temperature alteration of Ti- and Nb-phyllsilicates under laboratory conditions. in “Minerals as Advanced Materials I” S.V. Krivovichev ed., Springer-Verlag, Berlin, 143–151.
- Sheldrick, G.M. (2008): A short history of SHELX. *Acta Crystallogr.*, **A64**, 112–122.
- Sokolova, E. (2006): From structure topology to chemical composition. I. Structural hierarchy and stereochemistry in titanium disilicate minerals. *Can. Mineral.*, **44**, 1273–1330.
- Sokolova, E. & Cámara, F. (2017): The seidozerite supergroup of TS-block minerals: nomenclature and classification, with change of the following names: rinkite to rinkite-(Ce), mosandrite to mosandrite-(Ce), hainite to hainite-(Y) and innelite-1T to innelite-1A. *Mineral. Mag.*, DOI:10.1180/minmag.2017.081.010. in press
- Sokolova, E., Genovese, A., Falqui, A., Hawthorne, F.C., Cámara, F. (2017): From structure topology to chemical composition. XXIII. Revision of the crystal structure and chemical formula of zvyaginite, a seidozerite-supergroup mineral from the Lovozero alkaline massif, Kola peninsula, Russia. *Mineral. Mag.*, DOI:10.1180/minmag.2017.081.015. in press
- Utkin, M. Yu., Sukharev, V.N., Kirichek, O.P., Utkina, G.A., Lopatin, A.S., Kononova, L.N., Gordienko, A.V., Saykov, S., Mikhaelis, N.G. (1995): Report on preliminary exploration of eudyalite-loparite and eudyalite ores of Alluaiv locality of the Chinglusuay deposit in 1989–1992. Unpublished report, Revda, MGRE (in Russian).
- Vlasov, K.A., Kuz'menko, M.Z., Es'kova, E.M. (1966): The Lovozero Alkali Massif. Hafner Publishing Co., New York, 627.

Received 14 August 2017

Modified version received 20 October 2017

Accepted 31 October 2017